Smart Structures and Systems, Vol. 2, No. 3 (2006) 209-224
DOI: http://dx.doi.org/10.12989/sss.2006.2.3.209

The controllable fluid dashpot damper performance

Bijan Samali† and Joko Widjaja‡

Centre for Built Infrastructure Research, University of Technology, Sydney, P.O. Box 123, Broadway NSW 2007, Australia

John Reizes‡†

Faculty of Engineering, University of Technology, Sydney, Broadway NSW 2007, Australia

(Received March 27, 2004, Accepted March 14, 2006)

Abstract. The use of smart dampers to optimally control the response of structures is on the increase. To maximize the potential use of such damper systems, their accurate modeling and assessment of their performance is of vital interest. In this study, the performance of a controllable fluid dashpot damper, in terms of damper forces, damper dynamic range and damping force hysteretic loops, respectively, is studied mathematically. The study employs a damper Bingham-Maxwell (BingMax) model whose mathematical formulation is developed using a Fourier series technique. The technique treats this one-dimensional Navier-Stokes's momentum equation as a linear superposition of initial-boundary value problems (IBVPs): boundary conditions, viscous term, constant Direct Current (DC) induced fluid plug and fluid inertial term. To hold the formulation applicable, the DC current level to the damper is supplied as discrete constants. The formulation and subsequent simulation are validated with experimental results of a commercially available magneto rheological (MR) dashpot damper (Lord model No's RD-1005-3) subjected to a sinusoidal stroke motion using a 'SCHENK' material testing machine in the Materials Laboratory at the University of Technology, Sydney.

Keywords: fluid models; unsteady flow; dynamic range; damping; hysteresis.

1. Introduction

Due to the controllable fluids' unique rheological behavior capable of transforming from viscous liquid into semi solid state within a relatively short time, and due to its controllability under the influence of electric or magnetic fields, engineers have been utilizing these fluids to develop various locking, suspension and damper devices (Gavin, *et al*. 1996a-b, Makris, *et al*. 1996, Spencer, *et al*. 1997, Bölter and Janocha 1997, Kamath and Wereley 1997, McMahon and Makris 1997, Gorodkin, *et al*. 1998, Lee and Wereley 1999, Lindler and Wereley 1999, Park, *et al*. 1999, Sims, *et al*. 2000, Jansen and Dyke 2000, Bica 2002, Yang, *et al*. 2002, Janocha 2001, etc.). The use of this unique behavior is credited to Willis M. Winslow and Jacob Rabinov in relation to their patented works in the late 1940s as indicated in literature (Spencer, *et al*. 1997, Jansen and Dyke 2000). Among three operation modes,

† Professor, Corresponding Author, E-mail: Bijan.Samali@uts.edu.au
‡ jwidja@eng.uts.edu.au
‡† Adjunct Professor, E-mail: John.Reizes@uts.edu.au

i.e., pressure driven or flow mode, direct shear mode, and squeeze mode which are found in fluid devices, only the first two modes are mostly employed in device force generating mechanisms. Common types of pressure driven mode devices are dashpot dampers or actuator type dampers, shock absorbers and suspensions. Meanwhile clutches, brakes, controllable valves and shear mode dampers are classified as fluid direct shear mode devices. Moreover, the device force characterization is mostly carried out using a system identification method for mathematical modeling or by adjusting the relationship between device force and its response extracted from the experimental results in laboratory.

The current approaches include phenomenological modeling using Bouc-Wen model (Spencer, *et al*. 1997, Spencer, *et al*. 1998, Yang, *et al*. 2002), employing Chebyshev polynomials (Gavin, *et al*. 1996b), mechanical models (Chompucot 2000), rigid-viscoplastic material approximation or Buckingham's cubic equation (Makris, *et al*. 1996, Burton, *et al*. 1996, McMahon and Makris 1997), nonlinear viscoelastic-plastic model (Kamath and Wereley 1997), modified Buckingham's cubic equation (Sims, *et al*. 2000), a proposed polynomial model (Choi, *et al*. 2001), etc. Besides using experimental results, attempts by Gavin, *et al*. (1996a), Wereley, *et al*. (1998), Lee and Wereley (1999) and Widjaja *et al*. (2003) to characterize the relationship between device force and its response, mathematically, are mostly carried-out for quasi-static and fully developed steady conditions without emphasizing on force contribution of each parameter, namely, boundary conditions, viscous term, plug fluid and inertial term. To study force contributions to damper force, a damper Bingham-Maxwell (BingMax) model is employed in this study. The model comprises a non-linear equivalent viscous damping element and a spring mounted in series. The non-linear equivalent viscous damping forces are generated by Bingham fluid flowing through a parallel plate (duct) model in a shear-flow mode condition, while the spring, representing an accumulator, generates out of phase 'inelastic' damper forces. The study is based on the unsteady non-Newtonian flow and dynamic pressure gradient (Gavin, *et al*. 1996a). Although the simulation results are validated using the experimental results at device characterization stage, the study does not include the effects of friction between piston and casing, the carrier liquid type, the particle diameter, concentration, temperature and damper controllability performance. The controllability performance, adjustable with the supplied Direct Current (DC) level, requires control tests on the integrated models of MR dashpot damper and the structural prototype model.

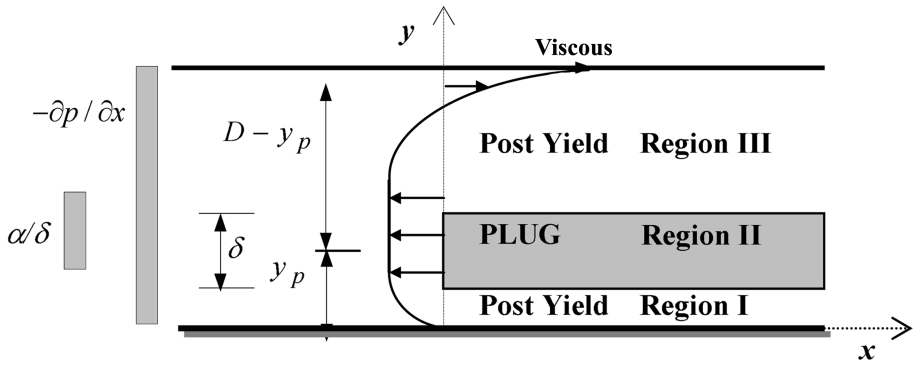

Fig. 1 Flow-field profile and 'uniform loadings' for pressure gradient and plug layer

2. Normalized non-Newtonian flow

Flow through the gap between piston and casing of a dashpot damper can be simulated as duct flow through a two parallel plate model with one moving boundary velocity U as shown in Fig. 1.

The flow, considered as a one dimensional non-Newtonian duct flow (Massey 1991) with constraint conditions such as: incompressible fluid, non-slip boundary, constant density, neglecting the presence of body forces and satisfying the principles of conservation of mass and momentum, is represented by the relationship below,

$$\rho(\partial\bar{u}/\partial\bar{t}) - \mu(\partial^2\bar{u}/\partial\bar{y}^2) = -\frac{\partial p}{\partial x} + \partial[\tau_y \mathrm{sgn}(\partial\bar{u}/\partial\bar{y})]/\partial\bar{y} \tag{1}$$

In the above equation, ρ is fluid mass density; $\bar{u}$ is flow velocity in x direction in the Cartesian (x-$\bar{y}$) coordinate system; $\bar{t}$ is temporal variable; $\partial p/\partial x$ is pressure gradient; τ_y is shear yield stress of fluid; μ is plastic viscosity of fluid; sgn is signum function and x, $\bar{y}$ are spatial coordinates of the Cartesian coordinate system. The above equation is derived using Bingham fluid model where fluid shear stress τ_{xy} is expressed as

$$\tau_{xy} = \tau_y \mathrm{sgn}(\partial\bar{u}/\partial\bar{y}) + \mu(\partial\bar{u}/\partial\bar{y}) \tag{2}$$

Introducing the normalized parameters given in Eq. (3) below, one can obtain the normalized Navier-Stokes' momentum equation as shown in Eq. (4)

$$y = \bar{y}/D \tag{3a}$$

$$u = \bar{u}/U_p \tag{3b}$$

$$t = \bar{t}/T_f \tag{3c}$$

$$T_f = \rho D^2/\mu \tag{3d}$$

$$R_U = \mu U_p/(\rho D) \tag{3e}$$

$$\frac{\partial u}{\partial t} - \frac{\partial^2 u}{\partial y^2} = -\frac{D}{\rho R_U}\frac{\partial p}{\partial x} + \frac{1}{\rho R_U}\partial\{\tau_y \mathrm{sgn}(\partial u/\partial y)\}/\partial y \tag{4}$$

In Eq. (3), R_U is the boundary velocity gradient induced fluid shear stress to density ratio; D is the size of annulus gap between piston and damper casing; T_f is the fluid time constant which varies from 0.003 to 0.24 for Magnetorheological (MR) fluids and from 0.001 to 0.12 for Electrorheological (ER) fluids, respectively. Both values hold for the gap size D in the range of 1 to 2.5 millimeters. The parameter U_p is the amplitude of piston head velocity.

3. Solutions of partial differential equation (PDE)

Using method of separation of variables, Eq. (4) can be separated into two ordinary differential equations (ODEs), by which the homogenous solution with the non-slip boundary conditions can be

obtained directly. The solution is taken as a product of two functions with each containing temporal and spatial terms only. The unknown constant associated with the homogenous solution is to finally be determined by imposing initial conditions to total velocity field contributed by boundary velocity, pressure gradient and fluid shear yield stress. On the other hand, the non-homogenous solution is solved by treating the pressure gradient, fluid shear yield stress (plug) and boundary velocity as 'constant terms'. The normalized boundary and initial conditions are as follows:

$$u_{(y=0,\,t)} = 0 \tag{5a}$$

$$u_{(y=1,\,t)} = \mathrm{Re}(\exp(i\lambda t)) \tag{5b}$$

$$u_{(y=t,\,0)} = 0 \tag{5c}$$

In Eq. (5), $\lambda = \omega T_f$ is the piston head normalized frequency and 'ω' is the piston head frequency. Eq. (5a) represents stationary boundary for damper casing, while Eq. (5b) is only used for moving boundary representing piston head, otherwise nil for homogenous, pressure gradient and fluid shear yield stress cases. Eq. (5c) corresponds to no fluid motion or at rest condition at initial time and is applicable to normalized unsteady flow velocity u.

Solving the homogenous and non-homogenous boundary cases of Eq. (4), with reference to normalized variables in Eq. (3), yields the following 'homogenous flow velocity u_h' and 'boundary induced flow velocity u_b' as follows:

$$u_h = \sum_{m=1}^{\infty} C_m \exp\{-(m\pi)^2 t\}\sin(m\pi y) \tag{6a}$$

$$u_b = \mathrm{Re}\{\sin(\phi y)/\sin(\phi)\}\mathrm{Re}(\exp(i\lambda t)) \tag{6b}$$

where C_m is integration constant of homogenous solution; Re stands for Real; Im stands for imaginary; $\phi = \sqrt{-i\lambda}$ and m is the subscript index (= 1,2,….~).

The pressure gradient and fluid shear yield stress are assumed to be piston head velocity dependent. Moreover, pressure gradient in Eq. (3) is treated as a constant with respect to ordinate y. As a result of treating Eq. (3) for steady state condition, the particular solution for the first RHS term of Eq. (3) represents the fully developed "pressure gradient-steady flow velocity u_p",

$$u_p = \sum_{m=1}^{\infty} B_m \sin(m\pi y) \tag{7}$$

$$B_m = -2\beta(1-\cos(m\pi))/(m\pi)^3 \tag{8a}$$

$$\beta = (\partial p/\partial x)D/(\rho R_U) = F/\{(\rho R_U)(\pi R^2 L/D)\} \tag{8b}$$

where B_m is the Fourier coefficient; β is the normalized pressure gradient; F is the dashpot damper force; R is the radius of piston head and L is the length of magnetic poles. In view of previous work of the authors (Widjaja, *et al*. 2003) the velocity profile for controllable fluid will transform into three layers when the applied pressure gradient is larger than the critical pressure gradient. The layers are two boundary adjacent fluid layers and one middle semi-solid or plug layer. Similar to the derivation of Eq. (7), the particular solution of "the plug inhibited flow velocity u_s" for the second RHS term of

Eq. (3), can be determined by using the conjugate beam analogy that the derivative of the fluid shear-yield stress is "a distributed loading α/δ" in the plug layer. In this case, the inertial term in conservation of momentum equation is neglected.

$$\frac{\partial^2(u_s)}{\partial y^2} = -\frac{\alpha}{\delta}(H_{(y-(y_p-\delta/2))}-H_{(y-(y_p+\delta/2))})\mathrm{sgn}\{\mathrm{Re}(\exp(i\lambda t))\} \tag{9}$$

In the above equation, $H_{(*)}$ is Heaviside's unit function, y_p is the normalized distance measured from the centroid of plug to the bottom plate, δ is the normalized plug thickness and α is the normalized fluid shear stress. These variables are defined below,

$$y_p = 1/2-\rho R_U/[\{(\partial p/\partial x)D\}(1-\delta)]|\mathrm{Re}(\exp(i\lambda t))| \tag{10a}$$

$$\delta = 2\tau_y/\{(\partial p/\partial x)D\} \tag{10b}$$

$$\alpha = 2\tau_y/(\rho R_U) \tag{10c}$$

Eq. (9) shows "a uniform loading" α/δ in the semi-solid region and "no loading" in the fluid regions acting on "a simple beam" as shown in Fig. 1. By applying the boundary conditions for velocity and compatibility conditions for velocity gradient at the fluid interface 'points' between liquid and semi-solid or plug layers, the "plug inhibited flow velocity u_s" can be obtained similar to 'bending moment' of a conjugate beam. The technique can avoid solving the integration constants resulting from mathematical double integration of discontinued 'loading'.

$$u_s = -\alpha\left\{\begin{array}{l}(y_p-1)y(H_{(y-0)}-H_{(y-(y_p-\delta/2))})+y_p(y-1)(H_{(y-(y_p+\delta/2))}-H_{(y-1)}) \\ +1/(2\delta)((y-y_p+\delta/2)^2+2y\delta(y_p-1))(H_{(y-(y_p-\delta/2))}-H_{(y-(y_p+\delta/2))})\end{array}\right\}\mathrm{sgn}\{\mathrm{Re}(\exp(i\lambda t))\} \tag{11}$$

For the ease of computation, Eq. (11) above is expanded into Fourier series as

$$u_s = \sum_{m=1}^{\infty}(A_m)\sin(m\pi y) \tag{12}$$

In Eq. (12), the coefficient A_m can be expressed as

$$A_m = (A_{1m}+A_{21m}+A_{22m}+A_{3m})*\mathrm{sgn}(\mathrm{Re}(\exp(i\lambda t))) \tag{13a}$$

where: $A_{1m} = -2(\alpha/2+\delta/(1-\delta)|\mathrm{Im}(\exp(i\lambda t))|)$

$$[m\pi(y_p-\delta/2)\cos\{m\pi(y_p-\delta/2)\}-\sin\{m\pi(y_p-\delta/2)\}]/(m\pi)^2; \tag{13b}$$

$$A_{21m} = -\alpha[2\sin\{m\pi(y_p+\delta/2)\}-4\sin(m\pi y_p)\sin(m\pi\delta/2)/(m\pi\delta)$$

$$-\delta m\pi\cos\{m\pi(y_p+\delta/2)\}]/(m\pi)^2; \tag{13c}$$

$$A_{22m} = -\{4\alpha(y_p-1)/(m\pi)^2\}\{\sin(m\pi\delta/2)(\cos(m\pi y_p)+m\pi y_p\sin(m\pi y_p))$$

$$-(m\pi\delta/2)\cos(m\pi\delta/2)\cos(m\pi y_p)\}; \tag{13d}$$

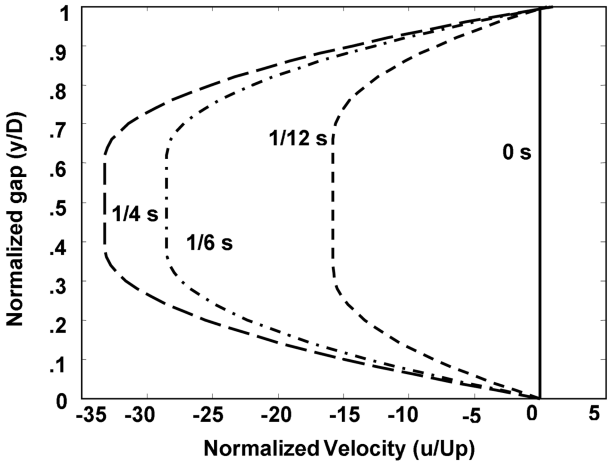

Fig. 2 Typical velocity profile for the case of $a = 50$, $f = 1$ Hz, $T_f = .003$ and $\alpha = 100$

$$A_{3m} = -(2/(m\pi)^2)(\alpha/2 - \delta/(1-\delta)|\mathrm{Im}(\exp(i\lambda t))|)$$
$$[m\pi(y_p + \delta/2 - 1)\cos\{m\pi(y_p + \delta/2)\} - \sin\{m\pi(y_p + \delta/2 - 1)\}] \quad (13e)$$

In view of Eqs. (6), (7), (8a), (12) and (13), the normalized unsteady flow velocity u through a parallel plate model for the condition of pressure gradient larger than critical pressure gradient (Widjaja, *et al.* 2003) can be derived after satisfying the initial condition in Eq. (5c):

$$u = \sum_{m=1}^{\infty} (A_m + B_m + C_m \exp\{-(m\pi)^2 t\})\sin(m\pi y) + \mathrm{Re}\{\sin(\phi y)/\sin(\phi)\}\mathrm{Re}(\exp(i\lambda t)) \quad (14)$$

where $C_m = -(A_m + B_m)$. Eq. (14) indicates that the solution for typical flow velocity profile across the parallel plate model as shown in Fig. 2, is influenced by inertial and initial conditions, boundary conditions, pressure gradient and fluid shear yield stress which are represented, respectively by C_m, u_b, B_m and A_m.

In the case of viscous dashpot damper with no electric or magnetic field applied, A_m equals to zero. Moreover, when used for flow mode dashpot dampers, the second term in Eq. (14) is dropped from the equation.

In order to observe the force characteristics of dashpot damper, the closed-form normalized damper force F^* of Bingham model is derived in view of Eq. (14).

$$F^* = \frac{\sum_{m=1}^{\infty} A_m[1 - \exp\{-(m\pi)^2 t\}]\{1 - \cos(m\pi)\}/(m\pi) + (\mathrm{Re}[\{1 - \cos(\phi)\}/\{\phi\sin(\phi)\}] + a/2)\mathrm{Re}(\exp(i\lambda t))}{2\sum_{m=1}^{\infty}[1 - \exp\{-(m\pi)^2 t\}]\{1 - \cos(m\pi)\}^2/(m\pi)^4} H_{(|\beta| - \alpha^*)} \quad (15)$$

In the above equation, $F^* = F/\{\rho R_U(\pi R^2 L/D)\} = \beta$; a is the damper geometrical factor $(R/(\gamma D))$; $\alpha^* = F_y/\{\rho R_U(\pi R^2 L/D)\}$; γ is the ratio of the gap annular perimeter with the piston perimeter and F_y is damper shear yield force. These normalized damper forces for various gap sizes with constraint of maximum piston head velocity gradient less than 'super slip velocity' $2\tau_y/\mu$ (Widjaja, *et al.* 2003) can

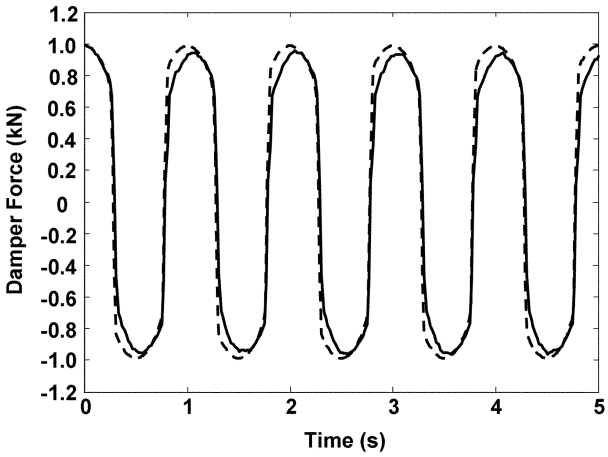

Fig. 3 Typical Simulation (--) versus Experimental results (—) for damper RD-1005-3 for 1 Hz, 1 Amp. and 12 mm stroke.

be typically shown in Fig. 3.

Moreover, Eq. (15) shows that the normalized damper force comprises of fluid shear yield stress induced force and viscous force, respectively, represented by A_m, the first numerator term and the numerator second term. This equation, and also indicates that damper damping characteristic is applicable with its second numerator term bounded larger than its first term as indicated by the Heaviside's unit function in Eq. (15). Furthermore, one can optimize the damper force by enlarging 'A_m', which means increasing the ratio of shear yield stress to gap size. This can be achieved by increasing electric or magnetic field intensity and/or by decreasing the gap between two dielectric plates or magnetic poles.

The transient contribution due to inertial and initial condition, represented by negative temporal exponential term, will decay in a short time during the damper operation. The roles of boundary condition and damper geometry in generating viscous force are represented respectively by the second numerator term. In view of Eq. (15), one can see that the viscous force increases as the ratio of piston head velocity to the squared gap size increases.

The decreasing gap size (or increasing the damper geometrical factor R/D) increases the damper force approximately linearly for the 'plug' flow and by more than two orders of magnitude larger (acting more like a viscous damper) than that of increasing piston head velocity with the same ratio. The effect occurs during post yield flow where the contribution of the viscous force becomes dominant especially at high piston head frequency or velocity. On the other hand the damper controllable force contributed by the pre-yield flow becomes dominant for the high yield stress controllable fluid damper or when operated at low piston head frequency or velocity. Furthermore, the normalized damper force in Eq. (15) for Bingham fluid model is represented by one mathematical function which can not describe the damper damping hysteretic behavior.

4. Damping characteristics of controllable dashpot damper

As Bingham fluid model used for dashpot damper (stated in Eq. (15) cannot describe the damping hysteretic behavior, the model is enhanced by installing an accumulator in series arrangement. The

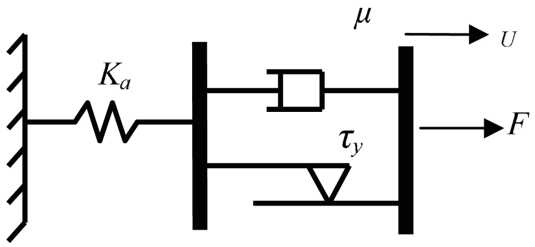

Fig. 4 Proposed BingMax device model

accumulator will act as spring with stiffness coefficient K_a. The new arrangement of damper representing a proposed Bingham-Maxwell (BingMax) device model as shown in Fig. 4 is able to generate the damping hysteretic behavior which is important if used as a control device.

The accumulator plays a role to split-up the function in Eq. (15) into four functions, illustrating the damper damping hysteretic curves. The piston velocity term contributed by the action of accumulator works at a different phase to those by the action of fluid. In this model, the normalized piston head velocity U/U_p is categorized into two conditions: for the case of F^* being less than F_y the normalized piston velocity is contributed by the accumulator only as in Eq. (16a). For the other case the normalized piston velocity is expressed as the summation of each normalized velocity contributed by plug, boundary effect, pressure gradient and accumulator (spring) which is further mathematically manipulated in relation to the normalized damper force F^* as in Eq. (16b).

$$dF^*/dt = KU/U_p \tag{16a}$$

$$dF^*/dt + (K/C)F^* = f(U/U_p, a, \lambda, A_m) \tag{16b}$$

The above equations hold for constant fluid shear yield stress where K is the normalized accumulator stiffness and C is the normalized viscous damping coefficient. The normalized viscous damping coefficient C of dashpot damper for the case of zero initial conditions can be derived by assuming the plug contribution or fluid shear yield stress is constant for each time step.

$$C = a/\left[4\sum_{m=1}^{\infty}[1-\exp\{-(m\pi)^2 t\}]\{1-\cos(m\pi)^2\}/(m\pi)^4\right] \tag{17}$$

$$K = K_a U_p T_f/(\rho R_U \pi R^2 L/D) \tag{18}$$

Furthermore, the Right Hand Side (RHS) term in Eq. (16) which represents the normalized forcing term can be expressed in relation to the fluid flow velocity as

$$f\left(\frac{U}{U_p}, a, \lambda, A_m\right) = K\left[\frac{2}{a}\sum_{m=1}^{\infty}A_m(1-\exp\{-(m\pi)^2 t\})\left(\frac{1-\cos(m\pi)}{m\pi}\right)\right.$$
$$\left.+\left(\mathrm{Re}\left(\frac{1-\cos(\phi)}{\phi\sin(\phi)}\right)+\frac{1}{2}a\right)\mathrm{Re}(\exp(i\lambda t))\right] \tag{19}$$

The normalized forcing term in the RHS of Eq. (19) is nonlinear and damper force dependent as

implicitly stated in A_m or specifically in δ and y_p. Treating Eqs. (16) as a linear ODE with constant coefficients for C, K and U/U_p for each time step and solving Eq. (16b) using MATLAB ODE45 or Euler method, the damper hysteretic behavior expressed as the damping force versus the piston head velocity relationship, can be obtained correspondingly as presented in Figs. (8a-l). The piston head displacement, which is also harmonic, can be derived using its velocity by which the damper energy dissipated can be computed as the area of hysteretic loop between damper force and piston head displacement. Further, the equivalent viscous damping can be determined as

$$\frac{C_{eq}}{\mu\pi L(R/D)^2} = \frac{2}{nt}\sum_{k=1}^{nt} F_k^* U_k \tag{20}$$

where nt is the number of time steps per cycle and k is the subscript index (1, 2, 3,…k,…., nt=2π/(ω Δt)).

5. Validation of the proposed BingMax damper model

To validate the performance of the proposed mathematical model with the test results, a series of experiment were set-up using a SHENCK material testing machine to drive a Lord Corp. manufactured 'Rheonetic' MR damper with part No. RD-1005-3, with an approximately 5 kN capacity load cell installed between the damper piston rod and the machine actuator as shown in Fig. 5. The test was conducted using sinusoidal excitations having frequencies of 0.5; 1.0; and 2.0 Hertz, while the supplied constant DC current levels to the damper varied correspondingly (0.0; 0.5; 1.0 and 2.0 Amperes). The damper fluid's rheological properties were characterized from the experimental results with the damper geometrical dimensions obtained by measurements. The damper has a piston diameter of 37.70 mm,

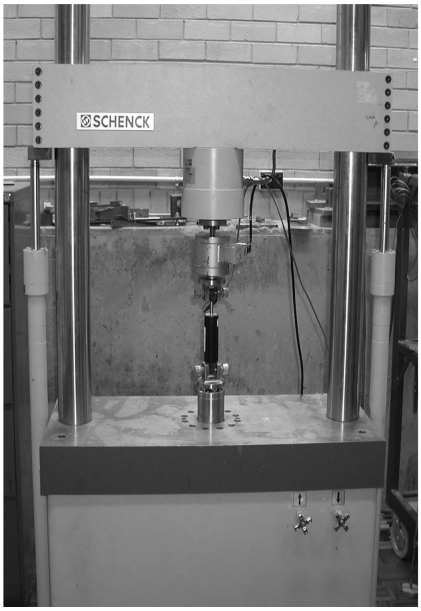

Fig. 5 Experimental Set-up for MR damper RD-1005-3 using a 'SCHENCK' test machine

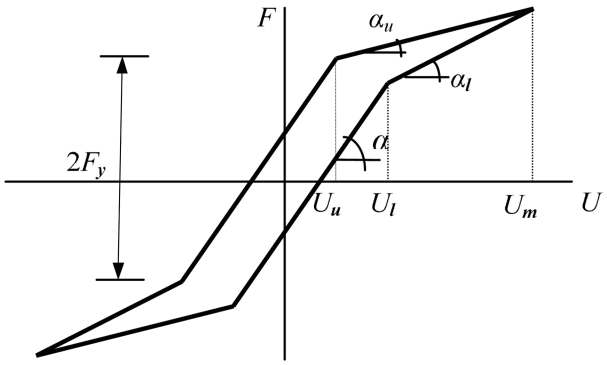

Fig. 6 Idealized MR damper hysteretic curve

1 mm gap thickness and 89.54 mm annular gap perimeter. The gap has two fixed magnetic poles (part of piston) 9 mm long through which the MR fluid flows in flow (valve) mode.

For the case of magnetized fluid condition, characterization of fluid shear yield stress, the fluid's rheological properties and accumulator elastic stiffness can be approximated using the measured slopes α, α_u, α_l, the measured piston velocity offsets U_u and U_l, depicted from the damper idealized hysteretic curve in Fig. 6.

$$\mu \cong D^2 \tan\left(\frac{\alpha_u + \alpha_l}{2}\right) / (12aA_pL) \tag{21a}$$

$$k_a \cong (4\pi f_p F_y) / |U_u - U_l| \tag{21b}$$

$$\tau_y \cong F_y D / (2A_pL) \tag{21c}$$

In the above equations, F_y is the measured damper shear force; α_u, α_l are the measured slopes of post-yield curves and U_u, U_l are velocity offsets at yield points. While for the case of non-magnetized fluid condition or zero DC current level, the dashpot damper is characterized similar to the viscous damper as shown in Fig. 7.

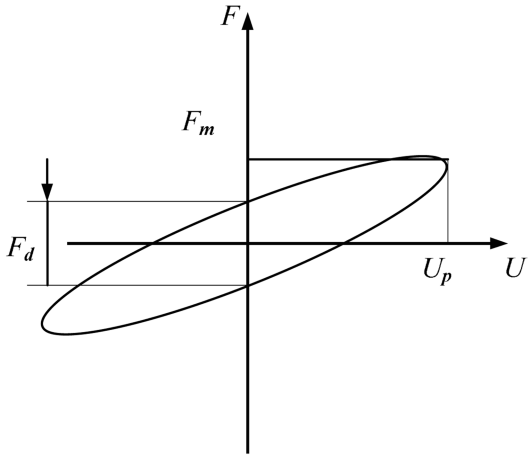

Fig. 7 Idealized viscous damper hysteretic curve

Table 1 Fluid shear yield stress, plastic viscosity and accumulator stiffness

Case	Freq. (Hz)	Current (Amp)	Stroke (mm)	τ_y (kPa.)	μ (Pa.s)	k_a (kN/m)
1	0.5	0.0	12.0	-	2.130	14.233
2		0.5		21.01	1.815	413.730
3		1.0		31.83	1.785	528.899
4		2.0		43.89	1.680	756.551
5	1.0	0.0	12.0	-	1.327	19.774
6		0.5		21.38	1.110	368.604
7		1.0		34.05	1.162	522.704
8		2.0		44.53	1.162	694.231
9	2.0	0.0	8.0	-	0.727	26.858
10		0.5		25.21	1.125	401.132
11		1.0		36.06	1.207	532.600
12		2.0		45.94	1.267	622.920

$$\mu_o = F_d / (6 U_p a \pi R^2 L / D^2) \tag{21d}$$

$$k_{ao} = 4\pi f_p F_m / U_p \tag{21e}$$

In Eqs. (21d-e), F_d and F_m are the measured offset damper force and maximum damper force, respectively. Characterization results can be seen in Table 1. Results indicate the nonlinearity of accumulator stiffness coefficient, fluid shear yield stress τ_y and post-yield viscosity 'μ'. The fluid shear yield stress is heavily current level rather than post yield viscosity dependent.

To build the signal based dashpot dampers, the damper performance can be expressed by the relationship of fluid shear yield stress and DC current level i as shown

$$\tau_y = 7.0578 i^3 - 32.76 i^2 + 59.682 i \quad \text{(kPa.)} \tag{22}$$

Validation of the proposed model using the experimental results and the input data in Table 1 can be seen in Figs. 8(a-l). In these figures, the dashed and solid lines correspond to damper forces obtained from the BingMax model and experiments, respectively.

6. Dynamic range of controllable dashpot dampers

One of the two most important parameters (besides the damper force) used for evaluation of damper performance (Carlson, *et al.* 1996, Gavin, *et al.* 1996, Yang G. 2001, Yang, *et al.* 2002) is dynamic range 'R_D', referred to also as control range of damper force which is defined as the force ratio between the maximum damper force when the damper is in 'ON' state (2.0 Ampere) and the maximum damper viscous force when the damper is in 'OFF' state (0 Ampere). The dashpot damper dynamic range, in view of Eq. (15) can be explicitly derived as:

$$R_D = \frac{\max\left|\sum_{m=1}^{\infty} A_m [1 - \exp\{-(m\pi)^2 t\}]\{1 - \cos(m\pi)\}/(m\pi) H_{(|\beta| - \alpha^*)}\right|}{\max\left|(\mathrm{Re}[\{1 - \cos(\phi)\}/\{\phi \sin(\phi)\}] + a/2)\mathrm{Re}(\exp(i\lambda t))\right|} + 1 \tag{23}$$

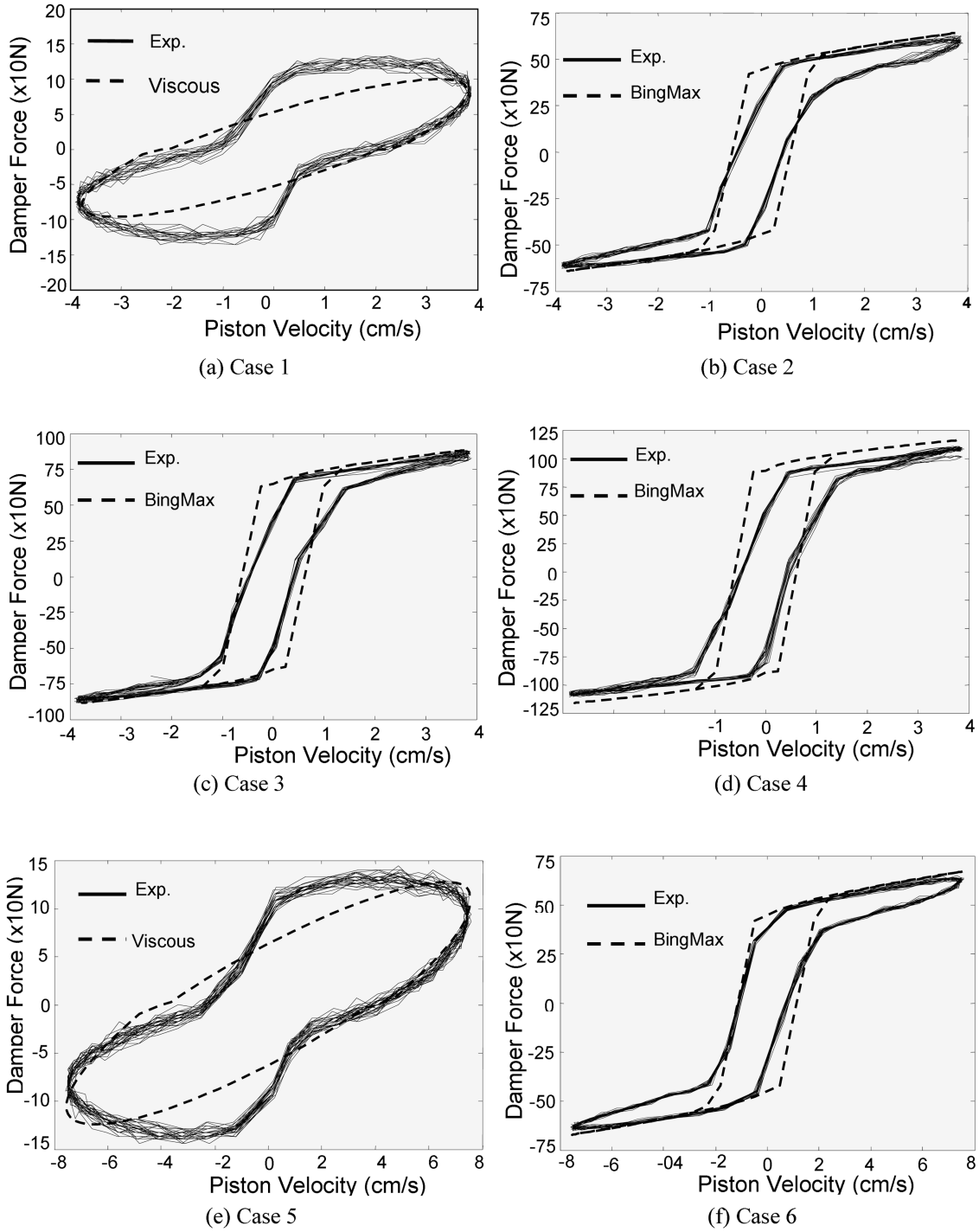

Fig. 8 Validation of BingMax model using Lord MR damper RD-1005-3: Experimental results (solid line), BingMax model (dashed line) corresponding to cases presented in Table 1

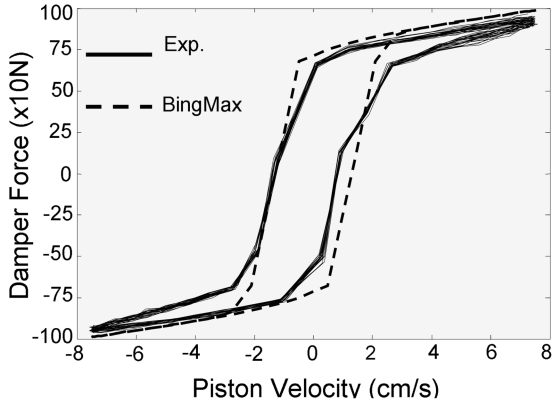

(g) Case 7

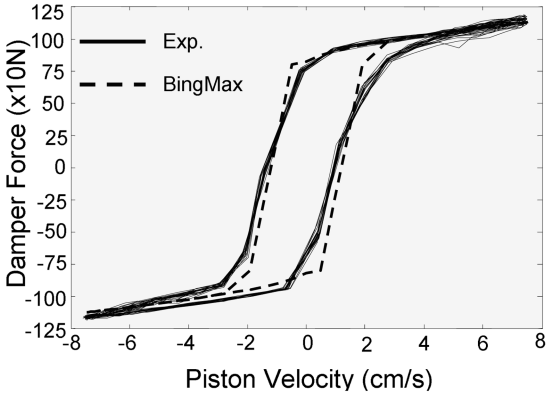

(h) Case 8

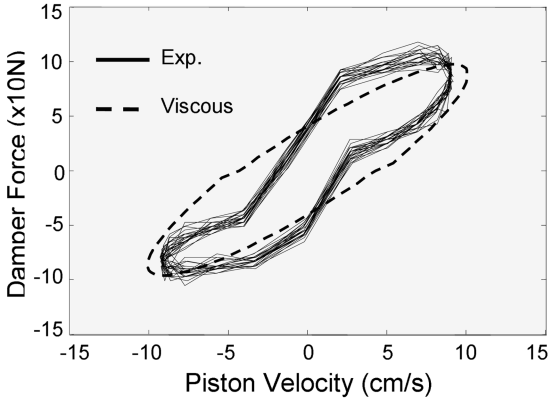

(i) Case 9

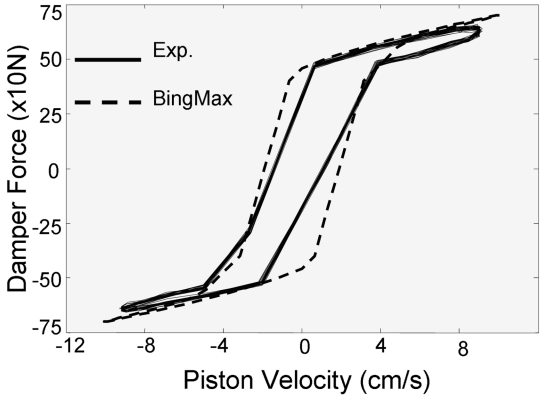

(j) Case 10

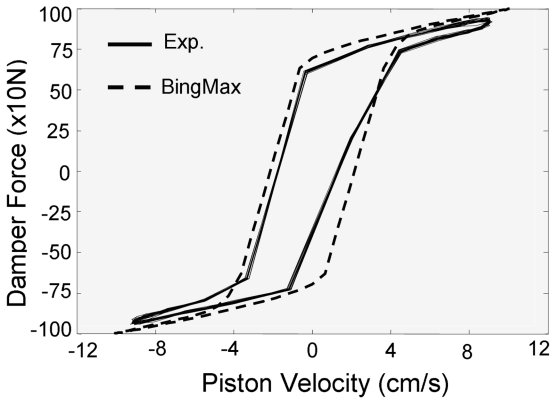

(k) Case 11

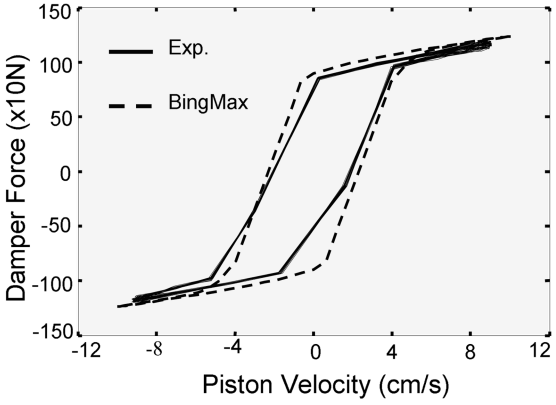

(l) Case 12

Fig. 8 Continued

One can observe that the dashpot damper dynamic range can be actively adjusted through 'A_m' or τ_y, which can be controlled by DC current level. Further, the numerical BingMax model shows an insignificant time delay in the damper operation especially for the large stiffness accumulator. In view

of Eq. (15), the decay time required to reach the quasi-steady condition for the dashpot damper can be approximated when the contribution of transient effects (exponential term) to damper force becomes equal or less than one percent, i.e.,

$$\sum_{m=1}^{\infty} \exp\{-(m\pi)^2 t\}(1-\cos(m\pi))/(m\pi) \leq 0.01 \tag{24}$$

Employing bisection method to find the root of Eq. (24) with the use of MATLAB version 6.1 release 12, one can obtain the approximate decay time t_d as

$$t_d \cong 0.42 T_f \tag{25}$$

The above solution indicates an approximate duration for fluid to reach its fully developed steady state which leads to a harmonic damper force. Furthermore, in view of Eq. (3d) it is shown that the smaller gap size causes significant reduction of decay time rather than having a larger plastic viscosity.

7. Discussions and conclusions

The formulation for controllable fluids' flow, as presented in this study shows that the flow can be represented explicitly by individual flows caused by inertial flow, boundary motions, generated pressure gradient and the presence of fluid plug generated by magnetic or electric fields. This approach is advantageous as it allows the study of the effect of each contributing factor to the damper force. The study firstly verifies the fluid velocity profile development as shown in Fig. 2. The higher will be the pressure gradient or damper force, as indicated by the development of post-yield viscous flow, when reducing the plug thickness inside the annulus gap. The analytically generated velocity profiles are based on the piston sinusoidal velocity. To validate the damper hysteretic force against the experimental results, a sinusoidal stroke motion was adopted as expressed by the formulations. Validation of the simulated BingMax damper model with experimental results was achieved typically for the case of 1 Hz. frequency, 1 Ampere constant DC supplied current with 12 mm piston stroke as presented in Fig. 3. The results indicate that the proposed damper BingMax model is in good agreement with the experimental results, with the exception that the simulation slightly over-estimates the maximum damper force. The root of this inaccuracy seems to lie in the characterization of the damper rheological properties and accumulator stiffness coefficients. Further works are still required to refine the characterization technique.

Without the presence of an accumulator, the damper cannot generate a significantly large force hysteretic behavior. One possibility is to place the accumulator and the dashpot component of damper in a serial arrangement. This arrangement leads to the so called BingMax damper model which in turn is capable of simulating the hysteretic behavior without affecting the magnitude of damper force. Validation of BingMax model for fluid dashpot dampers was carried-out using a 'Rheonetic' MR damper No. RD-1005-3 tested using sinusoidal excitation generated by a SHENCK material testing machine. Comparative results with those of BingMax models, employing the characterized fluid rheological properties and accumulator stiffness in Table 1, were presented in Figs. 8a-l. It can be seen that the BingMax models due to somewhat inaccurately characterized properties, are more rigid especially for low frequency, generally in good agreement but over estimating the damper force and the

damping/dissipated energy as indicated by the higher forces in Fig. 3 and larger width of hysteretic loops in Figs. 8a-l, respectively. In general the BingMax models show good results in comparison with the experimental results, however they require further softening to Bingham fluid model in order to be able to predict more accurately the damper hysteretic behavior. Moreover, the hysteretic loops for 'OFF' state or viscous condition indicate the presence of static friction forces which are not detected in characterization.

The transient effect on the damper dynamic ranges or forces due to initial condition occurs in a very short time and has no effect on dynamic range as indicated by the insignificant time delay in Eq. (25). This phenomenon also shows the insignificant fluid inertial effect passing through a small gap of two parallel magnetic poles or dielectric plates in a very short time, especially for low frequency mode of operation.

Acknowledgements

The authors gratefully acknowledge the support of UTS Centre for Built Infrastructure Research. In addition, the authors wish to thank my late colleague Dr. Lily Djajakesukma and Mr. Chris Chapman for their valuable assistance in conducting the experiments.

References

Bica, I. (2002), "Damper with magneto-rheological suspension", *J. Magnetism and Magnetic Materials*, **241**, 196-200.

Bölter, R. and Janocha, H. (1997), "Design rules for MR fluid actuators in different working modes", *SPIE* **3045**, 148-158.

Burton, S.A., Makris, N, Konstantopoulos, I. and Antsaklis, P.J. (1996), "Modeling the response of ER damper: phenomenology and emulation", *J. Eng. Mech.*, ASCE, **122**(9), 897-906.

Carlson, J.D., Catanzarite, D.M. and St. Clair, K.A. (1996), "Commercial magneto-rheological fluid devices", *Int. J. Modern Physics B* **10**(23-24), 2857-2865.

Chompucot, C. (2000), "Modeling ER and MR dampers", Master Thesis, Duke University, Durham, NC 27708.

Gavin, H.P., Hanson, R.D. and Filisko, F.E. (1996a), "Electrorheological dampers, Part I: analysis and design", *J. Appl. Mech.*, ASME, **63**(9), 669-675.

Gavin, H.P., Hanson, R.D. and Filisko, F.E. (1996b), "Electrorheological dampers, Part II: testing and modeling", *J. Appl. Mech.*, ASME, **63**(9), 676-682.

Gorodkin, S, Lukianovich, A. and Kordonski, W. (1998), "Magnetorheological throttle valve in passive damping systems", *Proc. 4th European and 2nd MIMR Conference*, 261-266.

Janocha, H. (2001), "Application potential of magnetic field driven new actuators", *Sensors and Actuators A*, **91**, 126-132.

Jansen, L.M. and Dyke, S.J. (2000), "Semi-active control strategies for MR dampers: A comparative study", *J. Eng. Mech.*, ASCE, **126**(8), 795-803.

Kamath, G.M. and Wereley, N.M. (1997), "Nonlinear modeling and performance prediction of electrorheological fluid dampers", *SPIE*, **3045**, 108-118.

Lee, D.Y. and Wereley, N.M. (1999), "Quasi-steady herschel-bulkley analysis of electro- and magneto- rheological flow mode dampers", *J. Intelligent Mater. Sys. Struct.* **10**(10), 761-769.

Lindler, J.E. and Wereley, N.M. (1999), "Double adjustable shock absorbers using electrorheological fluid", *Proc. 7th Int. Conf. on Electro-Rheological Fluids and Magneto-Rheological Suspensions,* Honolulu, Hawai, World Publishing Co. Pte, Ltd., Farrer Road, Singapore, 783-790.

Makris, N., Burton, S.A., Hill, D. and Jordan, M. (1996), "Analysis and design of ER damper for seismic protection

of structures", *J. Eng. Mech.,* ASCE, **122**(10), 1003-1011.
Massey, BS (1991), *Mechanics of Fluids,* Chapman & Hall, 2-6 Boundary Row, London.
McMahon, S. and Makris, N. (1997), "Large-scale ER-damper for seismic protection", *SPIE*, **3045**, 140-147.
Park, W.C., Choi, S.B. and Suh, M.S. (1999b), "Material characteristics of an ER fluid and its influence on damping forces of an ER damper Part II: damping forces", *Mater. Design*, **20**, 325-330.
Sims, N.D., Peel, D.J., Stanway, R., Johnson, A.R. and Bullough, W.A. (2000), "The electrorheological long-stroke damper: A new modelling technique with experimental validation", *J. Sound Vib*, **229**(2), 207-227.
Spencer, Jr., B.F., Dyke, S.J., Sain, M.K. and Carlson, J.D. (1997), "Phenomenological model of a magnetorheological damper", *J. Eng. Mech.*, ASCE, **123**(3), 230-238.
Spencer, Jr., B.F., Yang, G., Carlson, J.D. and Sain, M.K. (1998), "Smart dampers for seismic protection of structures: a full-scale study", *Proc. 2nd World Conf. on Structural Control*, Vol. 1, Kyoto, Japan, 417-426.
Wereley, N.M., Pang. L. and Kamath. G.M. (1998), "Idealized hysteresis modeling of electrorheological and magneto-rheological dampers", *J. Intelligent Mater. Sys. Struct.* **9**(8), 642-649.
Widjaja, J., Samali, B. and Li, J. (2003), "ER and MR duct flow in shear-flow mode using herschel-bulkley constitutive model", *J. Eng. Mech.*, ASCE, **129**(12), 1459-1465.
Yang, G. (2001), "Large-scale magnetorheological fluid damper for vibration mitigation: modeling, testing and control", PhD Dissertation, the University of Notre Dame, Notre Dame, Indiana.
Yang, G., Spencer, Jr., B.F., Carlson, J.D. and Sain, M.K. (2002), "Large-scale MR fluid dampers: modeling and dynamic performance considerations", *Eng. Struct.*, **24**, 309-323.

CK